JGR Planets

RESEARCH ARTICLE
10.1029/2022JE007220

Special Section:
ExoMars Trace Gas Orbiter - One Martian Year of Science

The Mars Oxygen Visible Dayglow: A Martian Year of NOMAD/UVIS Observations

L. Soret[1], J.-C. Gérard[1], S. Aoki[1,2,3], L. Gkouvelis[1,4], I. R. Thomas[2], B. Ristic[2], B. Hubert[1], Y. Willame[2], C. Depiesse[2], A. C. Vandaele[2], M. R. Patel[5], J. P. Mason[5], F. Daerden[2], J.-J. López-Moreno[6], and G. Bellucci[7]

[1]LPAP, STAR Institute, Université de Liège, Liège, Belgium, [2]Royal Belgian Institute for Space Aeronomy, Brussels, Belgium, [3]Department of Complexity Science and Engineering, Graduate School of Frontier Sciences, The University of Tokyo, Tokyo, Japan, [4]NASA/Ames Research Center, Mountain View, CA, USA, [5]School of Physical Sciences, The Open University, Milton Keynes, UK, [6]Instituto de Astrofisica de Andalucia-CSIC, Granada, Spain, [7]Istituto di Astrofisica e Planetologia Spaziali, Roma, Italy

Abstract The Ultraviolet and Visible Spectrometer Ultraviolet (UVIS UV) and Visible Spectrometer channel of the Nadir and Occultation for MArs Discovery spectrometer aboard the ExoMars Trace Gas Orbiter has made limb observations of the Martian dayglow during more than a Martian year. Two pointing modes have been applied: (a) In the inertial mode, the spectrometer scans the atmosphere twice down to near the surface and provides altitude profiles of the dayglow; (b) in the tracking mode, the atmosphere is scanned at varying latitudes at a nearly constant altitude through the entire observation. We present a statistical study of the vertical and seasonal distribution of the recently discovered oxygen green and red lines at 557.7 nm and 630 nm. It indicates that the brightness of the green line emission responds to changes in the Lyman-α flux. The peak altitude of the green line emission increases seasonally when the Sun-Mars distance decreases. The lower peak of the green line statistically drops by 15–20 km between perihelion and aphelion at mid-to high altitude. The main lower peak intensity shows an asymmetry between the two hemispheres. It is significantly brighter and more pronounced in the southern hemisphere than in the north. This is a consequence of the stronger Lyman-α solar flux near perihelion. The second component of the oxygen red line at 636.4 nm is also detected for the first time in the Martian atmosphere. A photochemical model is used to simulate the variations of the green dayglow observed along limb tracking orbits.

Plain Language Summary The Ultraviolet and Visible Spectrometer (UVIS) instrument aboard the ExoMars Trace Gas Orbiter made it possible to observe the visible emissions that occur on the dayside of the Mars atmosphere during more than a Martian year. Among them, the emissions of the oxygen called "green line" and "red line" (because of their wavelength of 557.7 nm and 630 nm, respectively), which are analyzed over time and can be used as proxies to study the changes in the upper atmosphere of Mars. We show that these emissions occur at higher altitudes and are brighter when Mars is closer to the Sun. We also show evidence of the presence of the second component of the red line at 636.4 nm, which confirms the identification of the recently discovered 630 nm emission. While the green line is composed of two peaks near 80 and 120 km, the red line limb brightness presents a broad peak near 140 km. Finally, we show that a photochemical model simulates the UVIS data very well.

Key Points:

- Nadir and Occultation for MArs Discovery/Ultraviolet and Visible Spectrometer limb observations of the green line dayglow show large seasonal variability in both the peak altitude and brightness
- We bring evidence of the presence of the second component of the oxygen red line at 636.4 nm
- Model simulations confirm that the Sun-Mars distance controls the altitude and the brightness of both oxygen emissions

Correspondence to:
L. Soret,
lauriane.soret@uliege.be

Citation:
Soret, L., Gérard, J.-C., Aoki, S., Gkouvelis, L., Thomas, I. R., Ristic, B., et al. (2022). The Mars oxygen visible dayglow: A Martian year of NOMAD/UVIS observations. *Journal of Geophysical Research: Planets*, *127*, e2022JE007220. https://doi.org/10.1029/2022JE007220

Received 9 FEB 2022
Accepted 12 MAY 2022

1. Introduction

The study of visible emissions in the upper atmospheres of terrestrial planets is necessary to get a better understanding of chemical processes and energy deposition. The first attempt to observe visible airglow on Mars was performed on the nightside with the spectrometer on board the Soviet MARS 3 spacecraft. No emission was detected and an upper limit of 50 rayleighs was set on the intensity of the OI green line nightglow at 557.7 nm (Krasnopolsky & Krysko, 1976). The lack of other planetary missions carrying dispersive instruments sensitive to visible radiation prevented detection of dayside emissions longward of 340 nm. Observations of visible Martian dayglow from the Earth's surface are strongly limited by the brightness of the nearby sunlit surface. Consequently, no oxygen emission has been observed on the dayside until the recent discovery by Gérard et al. (2020) of the green line dayglow with the Ultraviolet and Visible Spectrometer (NOMAD/UVIS) onboard the Trace Gas Orbiter (TGO) mission of the European Space Agency and ROSCOSMOS. TGO is on a quasi-circular

orbit inclined by 74° on the equator at about 400 km. The UVIS spectrometer is a component of the Nadir and Occultation for MArs Discovery (NOMAD) suite of instruments that was primarily designed to perform solar occultations and observe backscattered ultraviolet solar radiation.

The green line dayglow is characterized by the presence of two intensity peaks near 80 and 120 km. As was demonstrated by comparison with the O(^{1}S) production and loss processes simulated with the Photochemical Airglow Mars (PAM) model (Gkouvelis et al., 2018), the lower peak is the result of photodissociation of CO_2 into CO + O(^{1}S) by solar Lyman-α photons. The upper peak is generated by the same process resulting mainly from the interaction of extreme ultraviolet solar photons with CO_2. Gérard et al. (2021) have also recently detected the OI emission at 630 nm (the oxygen red line) by co-adding 777 NOMAD/UVIS dayside spectra collected between 100 and 200 km from April 2019 (MY 35, Ls = 11°) till October 2020 (MY 35, Ls = 293°). They found that the mean limb profile of [OI] 630 nm emission showed a broad intensity peak reaching 4.8 kR near 150 km. The average limb profile was successfully modeled and confirmed that the main sources of O(^{1}D) atoms are photodissociation of CO_2, photoelectron impact on O atoms, radiative relaxation from the O(^{1}S) atoms and O_2^+ dissociative recombination (Fox & Dalgarno, 1979; Raghuram et al., 2021). However, the second component of the ^{1}D –^{3}P transition expected at 636.4 nm could not be detected as the signal-to-noise ratio was too low with the available data set at the time. In this work we report presence of this second component and confirm the presence of [OI] red-doublet emission in the Martian upper atmosphere.

Furthermore, we describe the characteristics of the oxygen dayglow based on observations collected during more than a Martian year of UVIS measurements. The limb observations started on 24 April 2019 (MY 35, L_s = 15°) and this database extends until 31 December 2021 (MY 36, L_s = 150°). The entire database thus includes 137 orbits and 25,816 spectra. Aoki et al. (2022) focused on the retrievals of atmospheric density and temperature from the green oxygen dayglow measured by the inertial limb mode of UVIS. In this paper, we further investigate the variations of the green and red oxygen dayglow by using both inertial and limb tracking modes.

In Section 2, we describe the UVIS-TGO spectrometer and the observing modes applied to collect the dayglow spectra. The average dayglow spectrum deduced from these observations is showed in Section 3. In Section 4, we present the detection of the second component of the oxygen red line doublet. Section 5 is devoted to the generation of average limb profiles of the oxygen green and red lines while Section 6 focuses on their variability. Finally, in Section 7, some comparisons with model simulations are shown.

2. UVIS TGO Limb Observations

The aim of the NOMAD/UVIS spectrometer is mainly to perform solar occultations in the ultraviolet and observe backscattered solar radiation. The UVIS instrument can observe in limb and nadir observing modes (Patel et al., 2017; Vandaele, López -Moreno et al., 2018; Vandaele, Neefs, et al., 2018). The light passes through optical fibers to a plane grating and a collimating mirror on the 1024 × 256 pixel CCD detector. The circular field of view is 43 arcmin. The spectral resolution varies from 1.2 nm at 200 to 1.6 nm at 650 nm. The full spectrum is always observed in limb observations and the integration time is kept at 20 s for the airglow observations. In this study, we use data collected by UVIS in the special limb modes where the UVIS channel usually pointing to nadir is oriented toward the planetary limb (López-Valverde et al., 2018). They can either be “inertial” limb or “limb tracking” observations. In the first mode, the UVIS spectrometer scans the atmosphere from several hundreds of kilometers of altitude down to ∼80 km and then probes back up toward the upper atmosphere again. One observation is thus composed of two scans through the atmosphere (ingress and egress, see parabola-shapes in Figure 1a). As for the case of the special “limb tracking” mode, the UVIS boresight is constrained to remain close to a preset tangent altitude (±∼10 km) during a large fraction of the observations while a latitudinal scan through the atmosphere is performed (see horizontal lines in Figure 1a). Limb tracking observations started on 3 February 2021 (MY 35, L_s = 358°). This present tangent altitude is chosen close to the peak intensity of the [OI] 557.7 nm near 80 km or higher to optimize observations of the [OI] 630 nm and to search for other emissions.

In the data processing pipeline, the instrumental background or dark current (DC) in the CCD frame is first removed. Then, cosmic ray, anomalous and hot pixels are removed. Binning of 81 fully illuminated CCD lines is then performed to increase the signal-to-noise ratio of the spectrum. Finally, the count rate is converted in brightness units (kilorayleigh; 1 rayleigh = 10^6 photons cm^{-2} s^{-1} emitted in 4π steradians) based on laboratory and

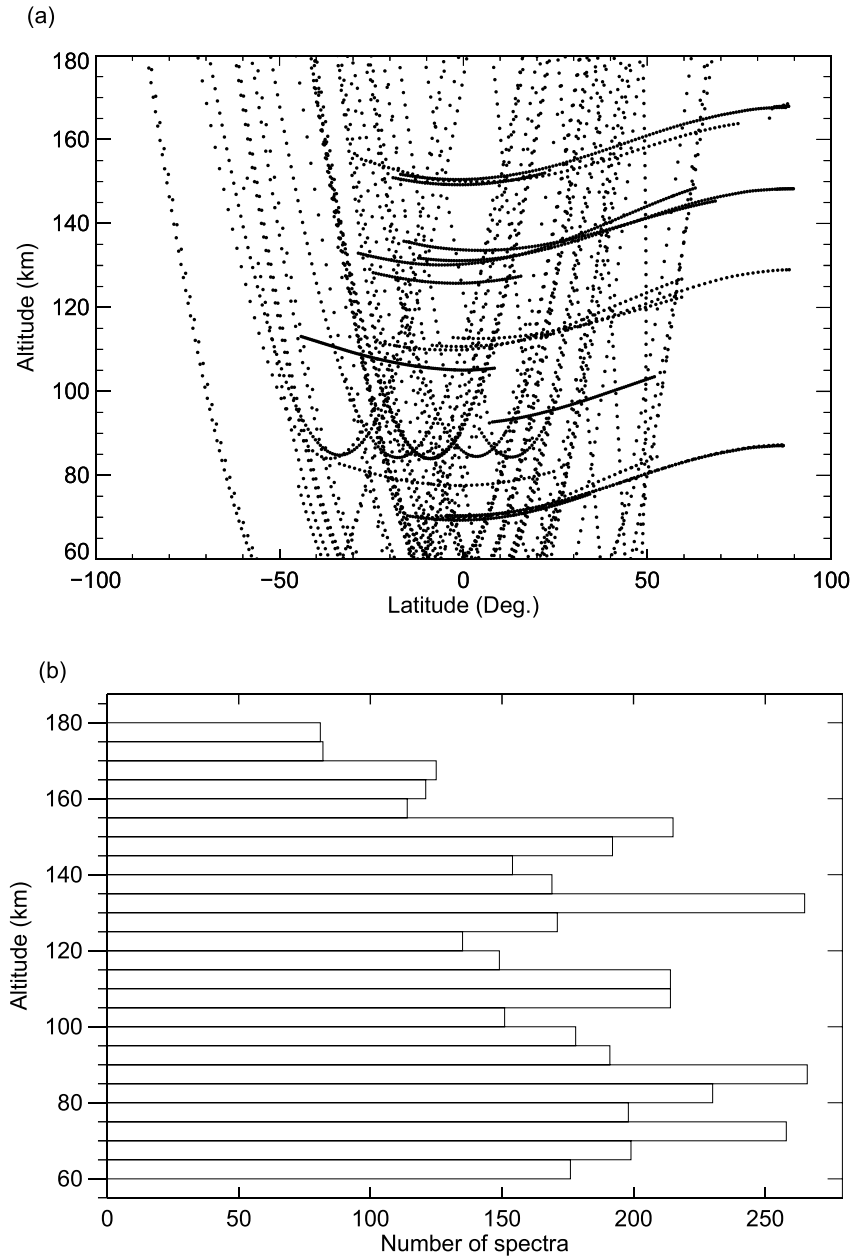

Figure 1. Limb data collected with Nadir and Occultation for MArs Discovery/Ultraviolet and Visible Spectrometer from 24 April 2019 (MY 35, L_s = 15°) to 31 December 2021 (MY 36, L_s = 150°) for solar zenith angles less than 70°. (a) Inertial limb observations are characterized by a parabola shape while limb tracking observations are represented by the nearly horizontal lines (nearly constant altitude of the tangent point during the observation). (b) Altitude distribution of the 4248 spectra grouped in 5 km bins.

in-flight measurements obtained during the calibration campaign. No stray light correction is required for these limb dayglow measurements but the noise removal is important as noisy pixel values can be several orders of magnitude larger than the faint dayglow signal. The statistical error on the brightness, as well as a systematic error can be associated with the uncertainties of the relative instrumental calibration estimated to be less than 10%.

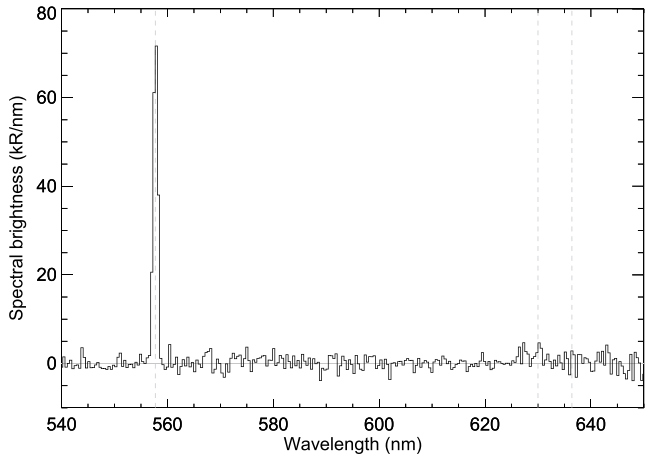

Figure 2. Average visible spectrum from Nadir and Occultation for MArs Discovery/Ultraviolet and Visible Spectrometer spectra obtained from 2531 spectra acquired between 75 and 140 km, for SZA <70° and all L_s. Vertical dashed lines represent the predominant oxygen green line at 557.7 nm and the much fainter red line doublet at 630–636.4 nm.

3. Mean NOMAD/UVIS Visible Dayglow Spectrum

We first compiled all spectra collected with a tangent point altitude between 60 and 180 km at a solar zenith angle (SZA) less than 70° to generate a unique database of spectra. Figure 1a shows the location in altitude and latitude of these 4248 acquired spectra, while Figure 1b represents their distribution in altitude. All altitudes are well covered, with at least one hundred spectra in each 5-km altitude bin below 170 km. It corresponds to a representative sample for a statistical study.

An average spectrum generated using all UVIS spectra between 75 and 140 km to limit contamination by solar scattered radiation at low altitude or sky background is shown as Figure 2. The background has been subtracted by using the average noise levels that were estimated in the [537.7–556.6], [558.8–577.70], [610.0–628.9], [631.1–650.0], [631.4–635.8] and [637.0–656.4]-nm wavelength intervals and connected together with linear fits. The oxygen green line is prominent at 557.7 nm and will be studied in Section 5.2. The red line doublet is much fainter at 630–636.4 nm. It will be described in Section 4. No other visible emission has been identified above the background noise.

4. Detection of the Red Doublet Component at 636.4 nm

As previously mentioned, the first detection of the red line dayglow (Gérard et al., 2021) could only identify the strongest component of the O ^{1}D-^{3}P transition at 630 nm. This electric dipole forbidden transition is actually composed of a doublet with a second component at 636.4 nm. This component could not be positively identified at the time of the discovery as the signal-to-noise ratio of the averaged spectrum was too low. Now, with the increased size of the limb dayglow database, we return to the search for the second component.

The red line doublet has been extensively observed in the Earth's airglow and auroral spectrum. The line intensity ratio R = I(630 nm)/I(636.4 nm) of the two components has been determined from both airglow measurements and from ab initio calculations. The theoretical estimations of R ranged from 2.997 to 3.10. Indeed, a detailed study of the ratio in the terrestrial nightglow observed with the Keck II telescope by Sharpee and Slanger (2006) led to a value of R = 2.997, in full agreement with the value from quantum mechanics calculation including relativistic effects by Storey and Zeippen (2000). This ratio was found consistent with an O(^{1}D) state radiative lifetime of 116 s. We thus conclude that the 636.4 nm component should be present in the NOMAD/UVIS spectra with a brightness close to 3 times less than the main 630 nm component.

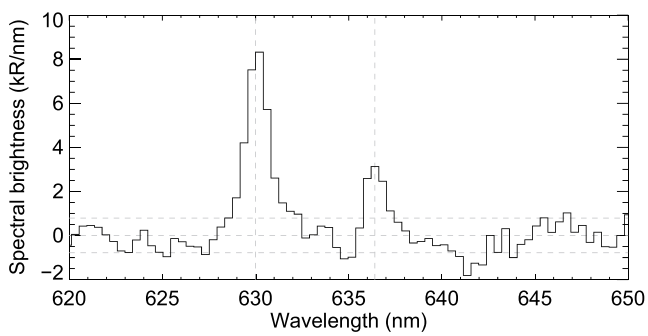

Figure 3. Average of 115 dayglow limb tracking spectra, essentially acquired during MY 36 (L_s = 0–150°). Spectra are corrected from background noise, as explained in Section 3. The two components of the O(^{1}D→^{3}P) transition can be seen. The vertical dashed lines indicate the wavelength of the two doublet components. The horizontal dashed lines show the ±1-σ deviation of the background noise in the spectral window.

In this study, we have accumulated observations in the limb tracking mode to search for the 636.4 nm component. The 630 nm emission is not always observed in the NOMAD/UVIS spectra: Its presence mainly depends on its brightness and on the altitude of the observations. The maximum of the 630 nm emission occurs at ∼140 km. To optimize the detection probability, we only consider those spectra collected with tangent altitudes between 100 and 180 km showing a signal-to-noise ratio at 630 nm higher than unity after background noise removal in the limb tracking mode. Figure 3 shows the average of 115 limb spectra matching these criteria. The mean 630.0 nm component brightness is 10.2 ± 3.5 kR, while that of the 636.4 nm line is 3.8 ± 2.7 kR, leading to a ratio 3.20 ± 0.50. This ratio is consistent with quantum mechanics calculations (Storey & Zeippen, 2000) and Earth's nightglow observations (Sharpee & Slanger, 2006). The presence of the second doublet component both corroborates the initial identification by Gérard et al. (2021) and confirms the constancy of the value of the ratio of the doublet components

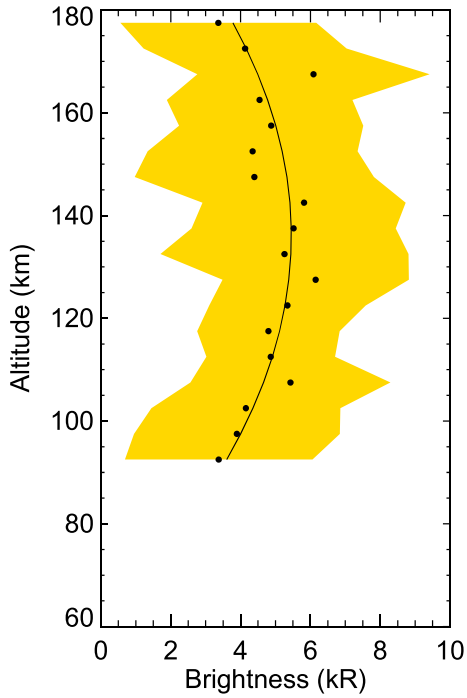

Figure 4. Average limb profile of the [OI] 630 nm dayglow (black dots) retrieved from 4248 spectra (see Figure 1) and best second order polynomial fit (black line). The emission maximum of the fit is located at 137.5 km and peaks at 5.3 kR. 1-σ uncertainties on the brightness estimates are colored in yellow.

in a physical and chemical planetary environment different from the Earth's conditions.

5. Limb Profiles

5.1. O(^{1}D) 630 nm Emission

Another improvement stemming from the increased number of limb scans is that the limb profile of the 630-nm emission and its variations may be described with increased accuracy. All the 4248 spectra collected both in the inertial and tracking limb modes have been corrected from the background noise (see Section 3) and grouped into 5 km bins (20 bins from 60 to 160 km) of altitude of the tangent point of the observation. The altitude distribution of the number of acquired spectra can be seen in Figure 1b. They all exceed 100 samples below 170 km. The mean brightness at 630 nm has then been retrieved for each of the 20 altitude bins, allowing the generation of a mean limb profile of the oxygen red line emission. The average limb profile of the 630 nm emission is presented in Figure 4. The best second order polynomial fit of the data is shown with a black line. Its maximum reaches 5.3 kR at 137.5 km. This result is in very good agreement with previous NOMAD/UVIS results from Gérard et al. (2021), based on a smaller number of observation than this study. Note that this average limb profile mixes up all latitudes, longitudes, SZA up to 70° and seasons. Because of the very faint signal of the red line, only a consequent accumulation of date makes it possible to generate a well-defined limb profile. Unfortunately, because we only have one Martian year of data for this study, red line limb profiles cannot be plotted over seasons.

5.2. 557.7 nm Limb Profile

Using the same 4248 spectra as for the red line, the global mean limb profile of the oxygen green line is shown in Figure 5. It confirms the characteristic shape presented by Gérard et al. (2020, 2021): A main peak located slightly below 90 km and a secondary peak near 120 km. Two different scale heights are readily seen: One between 95 and 110 km of about 13 km and a second one about 20 km above 125 km. Using a Chapman fit (Gérard et al., 2020; Gkouvelis et al., 2018; 2020b), temperatures can be derived from those scale heights (Jain et al., 2021). The corresponding temperatures are 93 and 143 K respectively. The lower peak intensity is 115 kR at 82.5 km, while the upper one is 55 kR at 117.5 km. These values are higher than those of Gérard et al. (2021) because the average Sun-Mars distance is smaller in this extended database than in the original report when the observations were made closer to aphelion. If the mesospheric scale height is extrapolated above 110 km and subtracted from the total signal (to remove the production of the upper peak caused by the photodissociation of CO_2 by solar Lyman-α photons), the secondary peak (generated by the interaction of extreme ultraviolet solar photons with CO_2) brightness reaches 22 kR. Note again that this average profile includes all latitudes, longitudes, solar zenith angles up to 70°, and seasons. Seasonal variations will be described in Section 6. The limb profile has been processed with an inversion method to retrieve the local volume emission rate (VER) at 557.7 nm and can be seen in Figure 5b. The method is based on an algorithm that solves the Abel inverse transformation (Hubert et al., 2022). The peak of the volume emission rate is located at 92.5 km, with a value of 0.13 ph cm^{-3} s^{-1}. The upper peak is also present near 125 km. Both peaks of the volume emission rate are located above those of the limb profile. This is a consequence of the integration along the line of sight that tends to smooth and decrease the apparent altitude of the local profile. An additional inflexion is observed near 107 km. This is probably an artifact due to the nearly imperceptible change of slope in the limb brightness profile at this altitude that can produce a sharp variation in the VER calculated by the Abel inversion (Hubert et al., 2016).

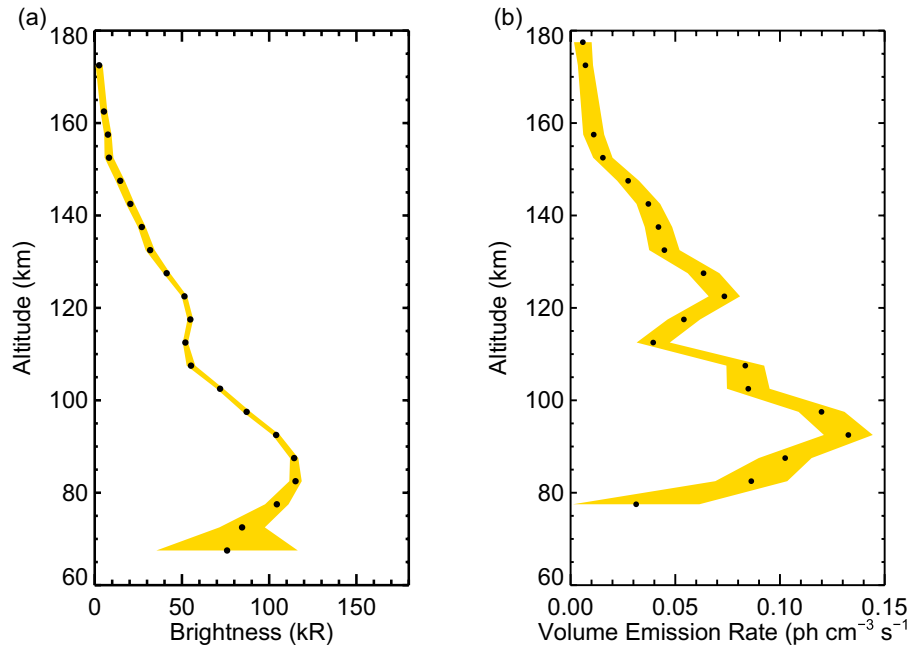

Figure 5. (a) global average limb profile of the [OI] 557.7 nm dayglow (black dots) retrieved from 4248 Nadir and Occultation for MArs Discovery/Ultraviolet and Visible Spectrometer spectra (see Figure 1). The emission peak is located at 82.5 km and reaches 115 kR. Uncertainties on the brightness estimates are colored in yellow. (b) Volume emission rate (VER) deduced from the profile shown in (a).

5.3. Oxygen Green Line and Ly-α

The upper peak of the oxygen green line is produced by the dissociation of CO_2 by solar extreme ultraviolet radiation, as described hereafter. The altitude of the lower 557.7 nm emission maximum is controlled by the content of the CO_2 column crossed by the solar Ly-α radiation to reach the peak. Gkouvelis et al. (2018) showed that the altitude of the lower peak of the [OI] 297.2 nm (and 557.7 nm) emission varies almost linearly with the logarithm of the CO_2 column density. Variations in altitude of the lower peak can thus be used to estimate altitudes changes of the pressure level in the mesosphere with latitude, season, and atmospheric dust load (Gkouvelis, Gérard, Ritter, et al., 2020). In contrast, model simulations indicate that the brightness of the lower peak depends on the Ly-α solar flux reaching the top of the Martian atmosphere. Here, instead of considering all the available spectra, we only use the intensity and altitude of the lower peak obtained with the 105 NOMAD/UVIS inertial limb profiles with a SZA less than 70° determined in Aoki et al. (2022). We compare it to the solar flux measured by the Extreme Ultraviolet Monitor onboard the Mars Atmosphere and Volatile Evolution (MAVEN) orbiter (Eparvier et al., 2015). EUVM measures the solar irradiance in the 0–7, 17–22 and 117–125 nm channels. Daily averages of calibrated solar spectra with a resolution of 1 nm are available from NASA's Planetary Data System website. The absolute calibration uncertainty at Ly-α is estimated to be on the order of 5%.

The comparison of the two quantities can be seen in Figure 6. The peak intensities retrieved from the UVIS inertial spectra have been corrected from the SZA dependence, using a 1/cos(SZA) relation appropriate for a Chapman layer. This correction tends to increase the brightness measured at high SZA values. They are shown with black dots in Figure 6a while the blue dots represent the Ly-α irradiance. Figure 6b shows the linear correlation of these two quantities with a Pearson coefficient of 0.70. According to the Fisher table for a population of 98 elements, the probability that the correlation is fortuitous is much less than 1%. The same comparison is done for the altitude of the lower (main) peak of the green line. Figure 6c shows the variations of the Ly-α solar flux (blue dots) together with the altitude of the green line lower peak (black dots). Here, the peak altitude is corrected from a dependence in SZA following the equation (Gkouvelis, Gérard, González-Galindo, et al., 2020): $z' = z - log\ [1/cos(SZA)] \times 7.1$, where z is the observed peak altitude, and z' is the corrected peak altitude. A correlation between the two quantities is observed and is confirmed by the correlation coefficient of 0.75 in Figure 6d. Once again, the probability that there is no correlation between the two quantities is less than 1%.

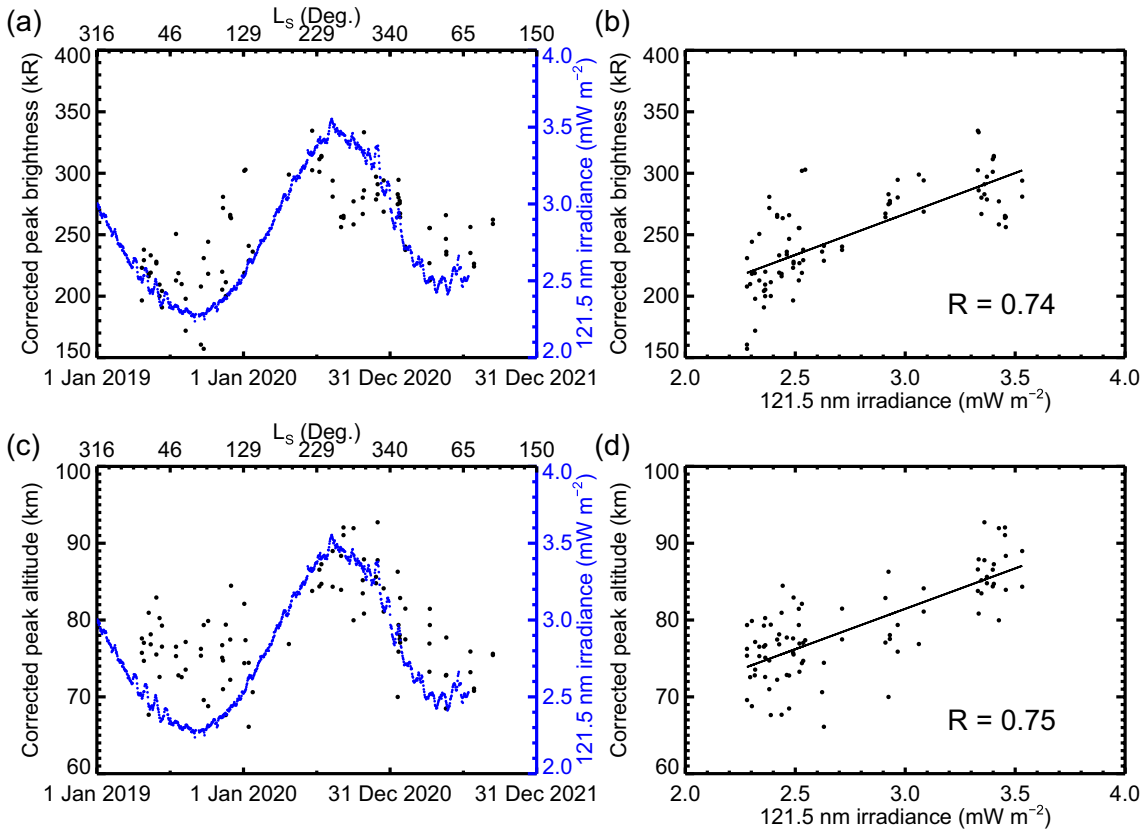

Figure 6. (a) Variation of the lower peak intensity of the oxygen green line along time (black dots). Intensities have been corrected from solar zenith angle (SZA) dependence. (b) A correlation with the Ly-α irradiance (blue dots) can be observed. (c) Variation of the lower peak altitude of the oxygen green line along time (black dots). Altitudes have been corrected from SZA dependence. (d) A clear correlation with the Ly-α irradiance (blue dots) can be observed.

However, contrary to the brightness that is directly produced by and proportional to the Ly-α intensity, the altitude of the green line emission is controlled by the CO_2 density. The Ly-α intensity is used as a proxy of the influence of the Sun-Mars distance on the peak altitude. These figures confirm the inflation of the atmosphere and the subsequent increase of the emission altitude when close to perihelion.

6. Seasonal Variations

Results presented in Section 5 mixed all limb scans, independently of the location and seasons of the observations. In this section, the acquired NOMAD/UVIS inertial and limb tracking data are now averaged according to those parameters.

Figure 7 shows limb profiles of the 557.7 nm emission generated according to L_s and latitude for solar zenith angles between 30 and 70°. They all show evidence of a double peak, especially in Figures 7a and 7b. The top panels (a and b) both represent averages in the equatorial region (30°S–30°N). The left curve is an average near aphelion ($L_s = 71° \pm 40°$, mean latitude of 1°N and mean SZA of 54°) while the right one is an average near perihelion ($L_s = 251° \pm 40°$, mean latitude of 4°S and mean SZA of 60°). The limb profile differences confirm that the emission occurs higher at perihelion than aphelion. As described by Gkouvelis, Gérard, González-Galindo, et al. (2020) for the [OI] 297.2 nm and Gérard et al. (2019) for the CO Cameron bands emissions, the increase of the thermospheric temperature and the expansion of the upper atmosphere near perihelion cause the isobar levels to move up. It is thus expected that the green line dayglow moves up to higher altitudes at this time of the year. Also, more photons reach the Martian atmosphere at perihelion and the brightest emission is thus expected during this period. However, the observed peak brightness is oddly less near perihelion than near aphelion.

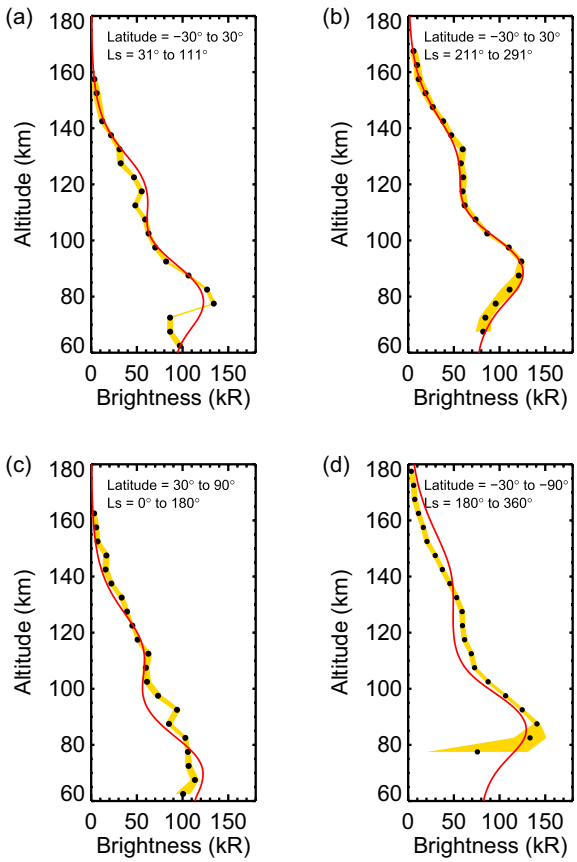

Figure 7. Averaged Ultraviolet and Visible Spectrometer limb profiles of the oxygen green line emission (black dots) acquired between 24 April 2019 (MY 35, $L_s = 15°$) and 31 December 2021 (MY 36, $L_s = 150°$). (a) Near aphelion in the equatorial region (based on a total of 825 spectra), (b) near perihelion in the equatorial region (based on a total of 337 spectra), (c) in northern spring and summer (based on a total of 954 spectra), (d) in southern spring and summer (based on a total of 465 spectra). Because observations end at $L_s = 150°$ for MY 36, only MY 35 data are shown in panel (b) and (d). The mean SZA of the four limb profiles vary between 55 and 60°. Uncertainties on the brightness estimates are colored in yellow. Simulations of the Photochemical Airglow Mars model for the same conditions are overplotted in red (see Section 7.2.3).

The lower panels of Figure 7 represent averages derived from summer in the northern (left) and southern (right) hemispheres. The two profiles exhibit very different shapes. The lower peak in the northern region is less pronounced than that of the southern hemisphere which is very well defined. The latter occurs at significantly higher altitudes than the former by 15–20 km. The lower peak intensity is much brighter and sharper in the southern hemisphere (141 kR) than in the Northern hemisphere (105 kR). Since the same season is analyzed in both cases (summer with mean latitudes of 52°N and 54°S, and SZA of 55° and 60°, respectively), the observed variations are essentially due to the variation of the Mars to Sun distance over a Martian year. No datapoint are shown below 75 km in Figure 7d because statistics was not good enough at that time and coordinates.

Average limb profiles have also been generated by bins of 5° of solar longitude (L_s) and latitude, mixing MY 35 and 36. The evolution of the peak altitude and brightness of the oxygen green and red emissions have been investigated. The variations of the averaged peak parameters are shown in Figure 8. Data have been collected during northern summer (top left part of each panel) and southern summer (bottom right part of each panel). Figure 8a represents the altitude of 557.7 nm emission peak, while its brightness is shown in Figure 8c. Note that a similar figure is shown in Figure 3c of Aoki et al. (2022) but Figure 8a is generated here with binned profiles to make comparison with those of the red line. The colors of the dots clearly show that the altitude of the green emission peak is higher during southern summer (86.3 km in average) than during northern summer (78.0 km). The peak brightness is 136.8 kR in the North and 132.2 kR in the South. In the 30° South and 30° North regions, the peak altitude of the green line is higher in the vicinity of perihelion ($L_s = 251°$), reaching 84.5 km, than near aphelion ($L_s = 71°$) where it occurs at 75.3 km. In contrast, the peak brightness of the green line emission is marginally less near perihelion than aphelion, with values of 132 and 136 kR, respectively. Variations can also be observed outside the equatorial regions, in agreement with Figure 7c and Figure 7d.

The right panels of Figure 8 represent the peak altitude and brightness of the red line. The same methodology as for the green line has been applied, but the low signal of the 630 nm emission and its broader distribution limit the detection of a clear peak in the limb profiles. Thus, data are binned over 15° of solar longitude and have to be taken cautiously. Similar to the green line, the red line peak occurs higher near perihelion (155.0 km) than near aphelion (123.3 km) while intensities are brighter near aphelion (10.4 kR) than near perihelion (7.0 kR).

Note that intensities shown in Figure 8 are somewhat higher than those of Figures 4 and 7 since Figure 8 focuses on peak statistics while previous figures mixed all the acquired observations.

7. Comparison With Model Simulations Along the Orbit

7.1. Limb Tracking Observations

We now focus on limb tracking observations, which provide a scan through the Mars atmosphere along latitudes at an almost fixed altitude (see Section 2 for more a more detailed description of the limb tracking mode of observation). The intensity variations of the 557.7 nm emission can be studied. Since the signal is very weak at 630 nm and can only be observed with an accumulation of spectra, the same analysis cannot be made for the oxygen red line. Figure 9 and 10 show the geometry (left panels) of the observations acquired on 16 February 2021 and 15 February 2021, respectively, near equinox ($L_s \approx 4°$) and the green line brightness extracted from each individual spectrum as a function of SZA, altitude and latitude (black dots, right panels). Using these two consecutive limb

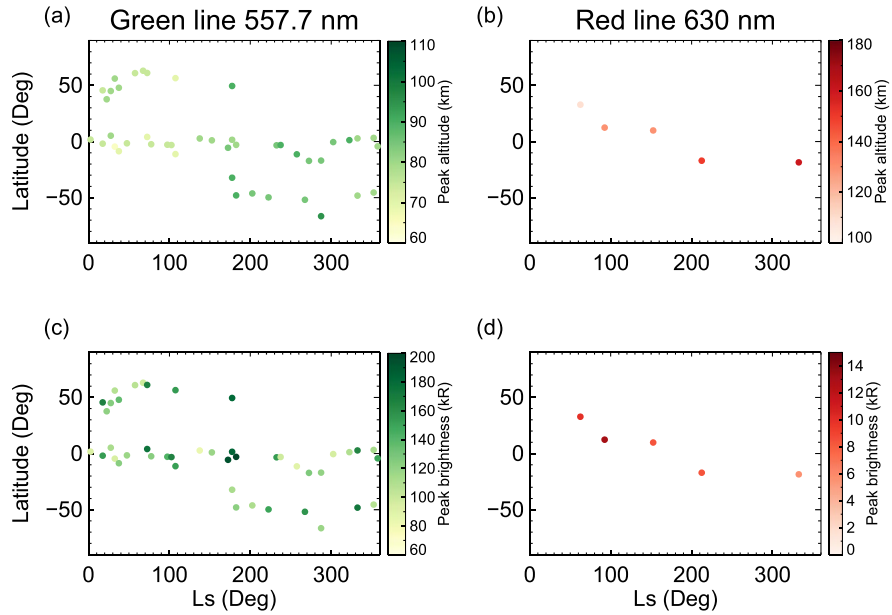

Figure 8. Variation of the peak altitude (top panels) and peak brightness (lower panels) of the oxygen green line (left panels) and red line (right panels) over seasons. Data points are generated using bins of 5° of solar longitude (L_s) and latitude for the green line. Bins of 15° of solar longitude are used for the red line.

tracking profiles enables us to analyze the lower peak of the green line at ∼80 km (Figure 9) and its upper peak at ∼120 km (Figure 10). Figures 9e and 10e shows that the 557.7 nm brightness changes over the observation, reaching a maximum at almost 20° of latitude, which corresponds to the smallest SZA point of the tangent point observed during this orbit. This can also be seen in Figure 10b: The brightness linearly increases with decreasing SZA, varying from ∼20 kR at SZA = 78° to a value of ∼60 kR at SZA = 60°. However, Figures 9d and 10d also shows an interesting result: The plots are divided into two branches, indicating that the same brightness is measured twice, but at different altitudes and latitudes. This is linked to the ingress and egress phases of the observation, where the atmosphere is scanned at two different latitudes and solar zenith angles.

7.2. The Photochemical Model

7.2.1. Comparison With a Full Limb Tracking Observation

Limb tracking observations are now compared with simulations made with the Photochemical Airglow Mars (PAM) model previously described by Gkouvelis et al. (2018), Ritter et al. (2019) and Gérard et al. (2020). In brief, the O(^{1}S) density is calculated at steady state as a function of altitude between 50 and 200 km. Photodissociation of CO_2 by solar Ly-α producing CO + O(^{1}S) is by far the dominant source process at the altitude of the lower peak. At higher altitude, dissociative recombination of O_2^+ and photoelectron impact on CO_2 contribute a few percent to the formation of O(^{1}S) atoms. Collisional deactivation by CO_2, O and CO competes with radiative relaxation of O(^{1}S) atoms at altitudes below ∼100 km. However, its efficiency remains less than 10% of the total radiative transition probability of 1.34 s above ∼70 km. Most recent cross sections, reaction coefficients and quantum efficiency were used. The neutral atmosphere density, temperature, and composition are taken from the Mars Climate Database (MCD) version 5.3. based on simulations from the Laboratoire de Météorologie Dynamique (LMD) (Forget et al., 1999; González-Galindo et al., 2009; Millour et al., 2015) for the appropriate Martian latitude, season, local time, and solar activity conditions. The Ly-α solar flux reaching Mars is obtained from the corresponding daily average measurement performed by the EUV monitor on board the MAVEN orbiter. Simulations made with this model provided very good agreement with [OI] 297.2 nm and 557.7 nm inertial limb intensity observations (Figures 9d, 9f and 10d–10f). In this section, we focus on the reliability of the model to match limb tracking observations.

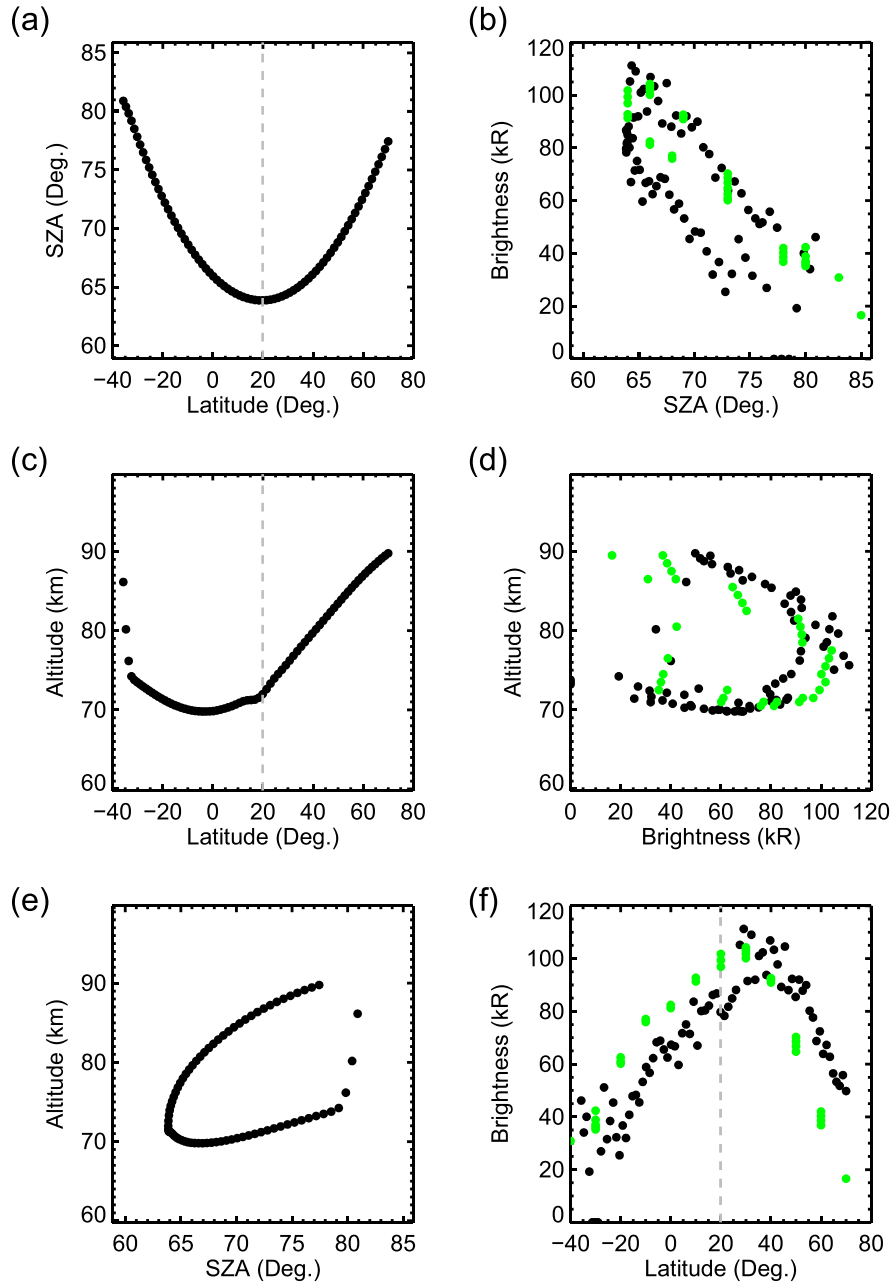

Figure 9. Nadir and Occultation for MArs Discovery/Ultraviolet and Visible Spectrometer limb tracking observation acquired on the 16 February 2021 ($L_s = 4°$) based on 77 spectra (black dots). The left panels represent the geometry of the observation, scanning the Mars atmosphere at almost fixed altitude ~80 km (lower peak of the green line) from 40°S to 70°N. The vertical dashed lines in panels (a, c, and f) represent the latitude where the solar zenith angle (SZA) is minimum. The right panels show the brightness evolution of the green line as a function of SZA, altitude and latitude. Model simulations are shown with green dots.

Simulations have been made for some of the geometrical data points of the 15/02/2021 and 16/02/2021 observations. The date of the observation, the SZA (every two degrees according to the observation geometry), and latitude (corresponding to the SZA regarding the geometry of the observation) are provided as inputs of the model. Altitude profiles of the green line volume emission rates are calculated for each individual spectrum. The volume emission rate is first integrated along the line of sight to simulate a UVIS limb observation (Hubert et al., 2022). Then, depending on altitude of the observations at specific SZA and latitude, the modeled limb profile is smoothed over ±10 km to account for the effect of the UVIS field of view. Each spectrum of the limb

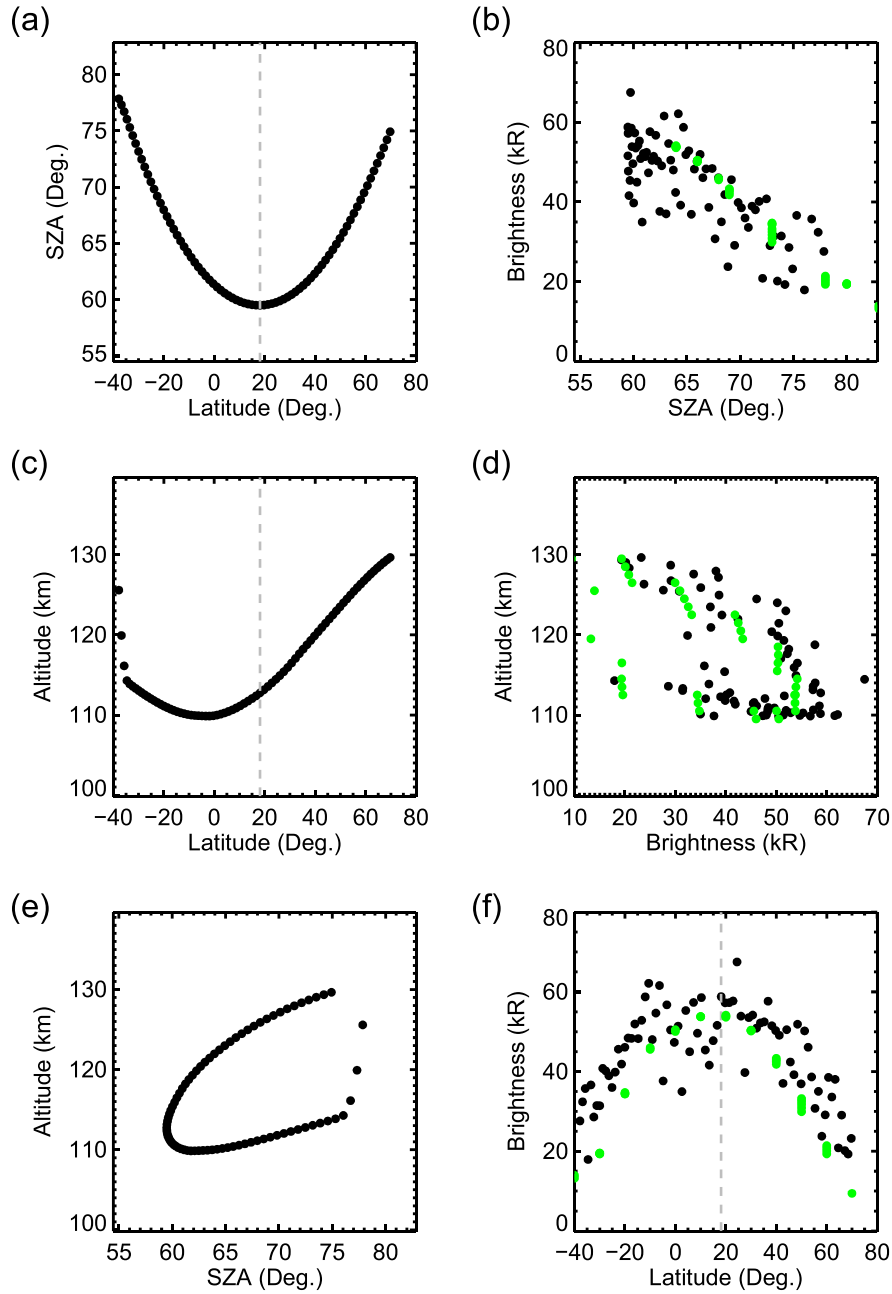

Figure 10. Nadir and Occultation for MArs Discovery/Ultraviolet and Visible Spectrometer limb tracking observation acquired on the 15 February 2021 ($L_s = 4°$) based on 78 spectra (black dots). The left panels represent the geometry of the observation, scanning the Mars atmosphere at almost fixed altitude ~120 km (upper peak of the green line) from 40°S to 70°N. The vertical dashed lines in panels (a and c) represent the latitude where the SZA is minimum. The right panels show the brightness evolution of the green line as a function of SZA, altitude and latitude. Model simulations are shown with green dots.

tracking UVIS observation is thus simulated in the appropriate observing conditions. Results of the simulations are shown as green dots on the right panels of Figures 9 and 10. The main features are well reproduced, including the presence of the two branches in Figures 9d and 10d. We thus confirm that the PAM model is highly reliable for local simulations as was shown by Gkouvelis et al. (2018, 2020a), Gérard et al. (2020, 2021), and Aoki et al. (2022). This implies that the photochemistry seems to be well understood and that the MCD values of the Mars atmosphere density are also adequate to predict the green line behavior.

Table 1
Nadir and Occultation for MArs Discovery/Ultraviolet and Visible Spectrometer Limb Tracking Observations and Comparison to Simulations of the Green Line Brightness

Date (YYYYMMDD)	Latitude (°)	Longitude (°)	SZA (°)	UVIS tangent point altitude (km)	UVIS maximum brightness (kR)	Model brightness (kR)
20210215	24.4	−146.1	59.7	114.4	68	66
20210216	29.1	−135.0	64.4	75.6	111	113
20210316	36.3	132.2	65.1	116.7	52	56
20210610	42.4	−178.9	56.5	78.2	140	134
20210610	29.4	96.9	56.1	115.0	75	66
20210708	51.2	−179.5	56.8	80.8	125	114
20210804	15.1	20.3	66.1	70.7	101	75

7.2.2. Comparison With Additional Limb Tracking Cases

A comparison with the PAM model of all individual spectra collected in the limb tracking mode would require us to be quite fastidious regarding our analysis. We limit ourselves to comparisons between the observations and the model results only for the maximum brightness of the 557.7 nm emission (i.e., one spectrum per limb tracking observation). Note that the maximum of the observed emission does not necessary imply that the actual local peak of the emission is detected. Again, we present here all limb tracking observations with a maximum occurring at a SZA less than 70°. When the tangent altitude of the line of sight is located near 80 km, the vicinity of the lower peak is observed, while the tangent point is closer to the upper peak when the line of sight scans the ∼115 km region. Results of the model simulations are given in Table 1 and compared with the limb tracking observations. The intensities simulated with PAM are very close to those observed by UVIS. Some differences can be noted though, but are easily explained. Indeed, the UVIS data show some intrinsic variability, contrary to the model results that are smoother. Therefore, the maximum UVIS brightness is not always perfectly located at the location predicted by the PAM model. For example, in Figure 10f, the maximum brightness is observed at 24°N latitude. However, a smoothing of the data would place the maximum at 19°N, and that is exactly where the model predicts it to be.

7.2.3. Comparison With Averaged Limb Profiles

Finally, model simulations have been performed for the mean results obtained for several latitudes and seasons as previously shown for the UVIS data in Figure 7. Results of these simulations are shown in red lines on those figures. Input parameters of each PAM model simulation corresponds to the average characteristics (latitude, SZA, longitude) of the average UVIS data used for each case. The simulated limb profile reproduces the observed brightness very well for every case. However, the CO_2 density from the MCD atmosphere that is used as an input parameter of the model was scaled so that the peak altitude retrieved from the simulations matches that of the observations. The applied scaling factors are 0.5, 1.4, 1.2 and 2.0 for Figures 7a–7d, respectively. The larger scaling factors occur for $L_s > 180°$. It thus seems that the MCD does not manage to quantitatively reproduce the increase in CO_2 density that leads to an upward displacement of the peak altitude when close to perihelion. Gkouvelis, Gérard, Ritter, et al. (2020) suggested that the model overestimates or underestimates the temperature vertical gradient. Also, they argued that the altitude of the homopause varies from 130 to 80 km as a function of L_s and SZA and season, so that the CO_2 mixing ratio is also variable at 120 km, leading to the discrepancy between the different pressure levels. However, the distance between the upper and the lower peaks is very well reproduced in every case.

8. Conclusions

Over one Martian year of limb observations have been analyzed to characterize the behavior of the oxygen green line and red line dayglow. A considerably large number of NOMAD/UVIS spectra have been been collected since the discovery papers of the green and red lines, covering different latitudes and solar zenith angles, The main results may be summarized as follows:

1. The second component of the red line doublet at 636.4 nm has been detected with a I(630.0 nm)/I(636.4 nm) intensity ratio close to 3, in agreement with theoretical predictions and terrestrial observations. This detection indirectly confirms the identification of the 630 nm red line.
2. The peak altitude of both the green and red oxygen emissions varies seasonally with the Sun-Mars distance. The main peak of the green line statistically drops by 15–20 km between perihelion and aphelion at mid to high altitude
3. The 557.7 nm peak intensity is asymmetric between the two hemispheres. It is significantly brighter (141 kR) and sharper in the southern hemisphere than in the north (105 kR), most likely as a consequence of the stronger Ly-α solar flux near perihelion.
4. The average limb distribution of the red line limb brightness is found to peak near 140 km, although the signal-to-noise ratio is considerably less than the green line. The difference with the green line distribution stems from the long (∼110 s) radiative lifetime of the O ^{1}D state, subject to collisional deactivation.
5. Both the main peak altitude and the intensity of the oxygen green line are correlated with the Ly-α solar flux reaching the planet.

On top of these observational results, comparison with model simulations show that the Photochemical Airglow Mars model correctly predicts the location of the green line peak, provides a good match to limb tracking observations of the green line intensity along the orbit and reproduces the brightness of that emission whatever the latitude, longitude, and season provided as input parameters. Only a moderate correction to the CO_2 density has to be applied to match the observed peak altitude, probably because standard averaged densities are used as input parameters or because the MCD model does not correctly reproduce the temperature vertical gradient. It remains important to keep track of these emissions over time so that the atmospheric variations along Martian years may be estimated, especially during dust storms.

The next step will be to perform the same analysis for ultraviolet emissions. In addition to determining their key parameters, it will be very important results to retrieve ratios between the ultraviolet and visible emissions.

Acknowledgments
The NOMAD experiment is led by the Royal Belgian Institute for Space Aeronomy (IASB-BIRA), assisted by Co-PI teams from Spain (IAA-CSIC), Italy (INAF-IAPS), and the United Kingdom (Open University). This project acknowledges funding by the Belgian Science Policy Office (BELSPO), with the financial and contractual coordination by the ESA Prodex Office (PEA 4000103401, 4000121493, 4000129686), by Spanish Ministry of Science and Innovation (MCIU) and by European funds under grants PGC2018-101836-B-I00 and ESP2017-87143-R (MINECO/FEDER), as well as by UK Space Agency. This work is supported by the UK Space Agency through grants ST/V002295/1, ST/V005332/1 and ST/S00145X/1 and Italian Space Agency through Grant 2018-2-HH.0. This research was supported by the Belgian Fonds de la Recherche Scientifique – FNRS under Grant No. 30442502 (ET_HOME). B. H. is supported by FNRS. The IAA/CSIC team acknowledges financial support from the State Agency for Research of the Spanish MCIU through the "Center of Excellence Severo Ochoa" award for the Instituto de Astrofísica de Andalucía (SEV-2017-0709). L. Gkouvelis is supported by the National Aeronautics and Space Administration. B. H. is supported by the Belgian Fund for Scientific Research (FNRS).

Data Availability Statement

The Mars Climate Database is available online at http://www-mars.lmd.jussieu.fr/mcd_python/ and the EUVM solar flux is available online at https://doi.org/10.17189/1517691. At the time of writing, SO occultation and UVIS occultation and nadir calibrated datasets are available on the ESA Planetary Science Archive at https://archives.esac.esa.int/psa/#!Table%20View/NOMAD=instrument for all data since the beginning of the nominal science mission (21 April 2018) up to 2020, with more recent data delivered regularly. LNO, UVIS limb, and calibration datasets for all channels are under preparation and are expected to be released to the public soon. The results retrieved from the NOMAD measurements used in this article are available on the BIRA-IASB data repository: https://repository.aeronomie.be/?doi=10.18758/71021077 (Soret & Vandaele, 2022).

References

Aoki, S., Gkouvelis, L., Gérard, J.-C., Soret, L., Hubert, B., Lopez-Valverde, M. A., et al. (2022). Density and temperature of the upper mesosphere and lower thermosphere of Mars retrieved from the OI 557.7 nm dayglow measured by TGO/NOMAD. *Journal of Geophysical Research: Planets*, *127*, e2022JE007206. https://doi.org/10.1029/2022JE007206

Eparvier, F. G., Chamberlin, P. C., Woods, T. N., & Thiemann, E. M. B. (2015). The solar extreme ultraviolet monitor for MAVEN. *Space Science Reviews*, *195*(1–4), 293–301. https://doi.org/10.1007/s11214-015-0195-2

Forget, F., Hourdin, F., Fournier, R., Hourdin, C., Talagrand, O., Collins, M., & Huot, J. P. (1999). Improved general circulation models of the Martian atmosphere from the surface to above 80 km. *Journal of Geophysical Research*, *104*(E10), 24155–24175.

Fox, J. L., & Dalgarno (1979). Ionization, luminosity, and heating of the upper atmosphere of Mars. *Journal of Geophysical Research*, *84*, A12.

Gérard, J. C., Aoki, S., Gkouvelis, L., Soret, L., Willame, Y., Thomas, I. R., et al. (2021). First observation of the oxygen 630 nm emission in the Martian dayglow. *Geophysical Research Letters*, *48*(8), e2020GL092334. https://doi.org/10.1029/2020GL092334

Gérard, J. C., Aoki, S., Willame, Y., Gkouvelis, L., Depiesse, C., Thomas, I. R., et al. (2020). Detection of green line emission in the dayside atmosphere of Mars from NOMAD-TGO observations. *Nature Astronomy*, *4*(11), 1049–1052.

Gérard, J. C., Gkouvelis, L., Ritter, B., Hubert, B., Jain, S. K., & Schneider, N. M. (2019). MAVEN-IUVS observations of the CO_2^+ UV doublet and CO Cameron bands in the Martian thermosphere: Aeronomy, seasonal, and latitudinal distribution. *Journal of Geophysical Research: Space Physics*, *124*(7), 5816–5827.

Gkouvelis, L., Gérard, J. C., González-Galindo, F., Hubert, B., & Schneider, N. M. (2020). Isobar altitude variations in the upper mesosphere observed with IUVS-MAVEN in response to martian dust storms. *Geophysical Research Letters*, *47*(12), e2020GL087468. https://doi.org/10.1029/2020gl087468

Gkouvelis, L., Gérard, J. C., Ritter, B., Hubert, B., Schneider, N. M., & Jain, S. K. (2018). The O(^{1}S) 297.2-nm dayglow emission: A tracer of CO_2 density variations in the martian lower thermosphere. *Journal of Geophysical Research: Planets*, *123*(12), 3119–3132.

Gkouvelis, L., Gérard, J. C., Ritter, B., Hubert, B., Schneider, N. M., & Jain, S. K. (2020). Airglow remote sensing of the seasonal variation of the martian upper atmosphere: MAVEN limb observations and model comparison. *Icarus*, *341*, 113666.

González-Galindo, F., Forget, F., López-Valverde, M. A., Angelats i Coll, M., & Millour, E. (2009). A ground-to-exosphere martian general circulation model: 1. Seasonal, diurnal, and solar cycle variation of thermospheric temperatures. *Journal of Geophysical Research*, *114*(E4).

Hubert, B., Munhoven, G., Moulane, Y., Hutsemekers, D., Manfroid, J., Opitom, C., & Jehin, E. (2022). Analytic and numerical methods for the Abel transform of exponential functions for planetary and cometary atmospheres. *Icarus*, *371*, 114654. https://doi.org/10.1016/j.icarus.2021.114654

Hubert, B., Opitom, C., Hutsemékers, D., Jehin, E., Munhoven, G., Manfroid, J., et al. (2016). An inversion method for cometary atmospheres. *Icarus*, *277*, 237–256. https://doi.org/10.1016/j.icarus.2016.04.044

Jain, S. K., Soto, E., Evans, J. S., Deighan, J., Schneider, N. M., & Bougher, S. W. (2021). Thermal structure of Mars' middle and upper atmospheres: Understanding the impacts of dynamics and solar forcing. *Icarus*, *114703*. ISSN 0019–1035. https://doi.org/10.1016/j.icarus.2021.114703

Krasnopolsky, V. A., & Krysko, A. A. (1976). On the night airglow of the Martian atmosphere. XVI. In *Proceedings of working groups on physical sciences, and symposium and workshop on results from coordinated upper atmosphere measurement programs* (pp. 1005–1008). Akademie-Verlag GmbH.

López-Valverde, M. A., Gérard, J. C., González-Galindo, F., Vandaele, A. C., Thomas, I., Korablev, O., et al. (2018). Investigations of the Mars upper atmosphere with ExoMars trace gas orbiter. *Space Science Reviews*, *214*(1), 29.

Millour, E., Forget, F., Spiga, A., Navarro, T., Madeleine, J. B., Montabone, L., et al. (2015). *The Mars Climate Database (MCD Version 5.2)* (Vol. 10). EPSC abstract 2015-438.

Patel, M. R., Antoine, P., Mason, J., Leese, M., Hathi, B., Stevens, A. H., et al. (2017). NOMAD spectrometer on the ExoMars trace gas orbiter mission: Part 2—Design, manufacturing, and testing of the ultraviolet and visible channel. *Applied Optics*, *56*(10), 2771–2782. https://doi.org/10.1364/AO.56.002771

Raghuram, S., Jain, S. K., & Bhardwaj, A. (2021). Forbidden atomic oxygen emissions in the Martian dayside upper atmosphere. *Icarus*, *359*, 114330. https://doi.org/10.1016/j.icarus.2021.114330

Ritter, B., Gérard, J.-C., Gkouvelis, L., Hubert, B., Jain, S. K., & Schneider, N. M. (2019). Characteristics of Mars UV dayglow emissions from atomic oxygen at 130.4 and 135.6 nm: MAVEN/IUVS limb observations and modeling. *Journal of Geophysical Research: Space Physics*, *124*, 4809–4832. https://doi.org/10.1029/2019JA026669

Sharpee, B. D., & Slanger, T. G. (2006). O(^{1}S→^{1}D,^{3}P) 630.0, 636.4, and 639.2 nm forbidden emission line intensity ratios measured in the terrestrial nightglow. *The Journal of Physical Chemistry A*, *110*(21), 6707–6710.

Soret, L., & Vandaele, A. C. (2022). Dataset of the retrieved oxygen green and red lines from TGO/NOMAD/UVIS dayside limb observations, presented in Soret et al., 2022 [Data set]. Royal Belgian Institute for Space Aeronomy. https://doi.org/10.18758/71021077

Storey, P. J., & Zeippen, C. J. (2000). Theoretical values for the [O III] 5007/4959 line-intensity ratio and homologous cases. *Monthly Notices of the Royal Astronomical Society*, *312*(4), 813–816. https://doi.org/10.1046/j.1365-8711.2000.03184.x

Vandaele, A. C., López -Moreno, J.-J., Patel, M. R., Bellucci, G., Daerden, F., Ristic, B., et al. (2018). NOMAD, an integrated suite of spectrometers for the ExoMars Trace Gas Mission: Technical description, science objectives, and expected performance. *Space Science Reviews*, *214*(5). https://doi.org/10.1007/s11214-018-0517-2

Vandaele, A. C., Neefs, E., Drummond, R., Thomas, I. R., Daerden, F., López-Moreno, J. J., et al. (2018). Science objectives and performances of NOMAD, a spectrometer suite for the ExoMars TGO mission. *Planetary and Space Science*, *119*, 233–249. https://doi.org/10.1016/j.pss.2015.10.003